STM JOURNALS

Journal of
Catalyst & Catalysis

ISSN: 2349-4344
Volume 12, Issue 1, 2025
January—April
DOI (Journal): 10.37591/JoCC

https://journals.stmjournals.com/jocc

Research JoCC

A Non-hydrotreated Feedstock's Polyaromatic Cracking Under FCC Industrial Operating Conditions Using an Equilibrium Catalyst

Seybou Yacouba[1], Hua Ye[2], Chongwen Jiang[3], Alberto Afonso Fernandes Tomás[4], Kianre-Djo-Tana Rissimbaye Frederic[5]

Abstract

Catalytic cracking of non-hydrotreated atmospheric residue's main polyaromatic hydrocarbon (PAHs) in the presence of an equilibrium catalyst was investigated under industrial operating conditions. During the fluid catalytic cracking process, the catalyst that presented the key factor in hydrocarbon cracking (aromatic by hydrogen transfer reaction) quickly deactivated and compromised the process's performance due to its acid surfaces and pores covered by the polyaromatic species. A deep study of the catalyst behavior was carried out at different steps of the process (fresh, regenerated, and spent states) using powerful spectroscopy methods including. Barrett–Joyner–Halenda (BJH), Fourier-transform infrared (FTIR), and nuclear magnetic resonance spectroscopy (NMR^{13}C). The gas chromatography−mass spectrometry (GC-MS) technique was employed to study the effect of the catalyst (hydrogen donor) on the polyaromatic hydrocarbon conversions in the feedstocks and naphtha as the reaction main product. BJH, Pyridine-FTIR, and NMR^{13}C results indicated that the deposition of carbon species (aromatic) on the catalyst's active surfaces and pores was the main cause of its deactivation. The GC-MS technique revealed twelve PAHs in the studied samples, but only Fluorene, Phenanthrene, Benzo(k) fluoranthene, and Xylene were affected or converted over catalyst due to the catalyst selectivity aspect. In addition, the cracking mechanism of Fluorene (four-rings) and Phenanthrene(three-rings) was also detailed as the main PAHs in the feedstock.

Keywords: Non-hydrotreated feedstock, PAHs, FCC, Catalyst, hydrogen transfer

***Author for Correspondence**
E-mail: yehua308@csu.edu.cn

[1]PhD Student, Department of Chemical Engineering and Technology, School of Chemistry and Chemical Engineering, Central South University, Changsha, China
[2,3]Professor, CSU, Department of Chemical Engineering and Technology, School of Chemistry and Chemical Engineering, Central South University, Changsha, China
[4,5]Master Student, CSU, Department of Chemical Engineering and Technology, School of Chemistry and Chemical Engineering, Central South University, Changsha, China

Received Date: October 02, 2025
Accepted Date: January 05, 2025
Published Date: January 10, 2025

Citation: Seybou Yacouba, Hua Ye, Chongwen Jiang, Alberto Afonso Fernandes Tomás, Kianre-Djo-Tana Rissimbaye Frederic. A Non-hydrotreated Feedstock's Polyaromatic Cracking Under FCC Industrial Operating Conditions Using an Equilibrium Catalyst. Journal of Catalyst & Catalysis. 2025; 12(1): 33–44p.

INTRODUCTION

The major challenge in refining heavy oil (hydrotreated feedstock or non-hydrotreated feedstock as in our case) in the industrial FCC process is related to maintaining a long cycle life of the catalyst and avoiding its fast deactivation due to many factors including aromatic components. In addition, increasing reaction product amounts and qualities required the cracking of long chains to valuable olefine and smaller chains. To achieve these two major objectives, it is imperative to use a selective catalyst that can decompose the long chain and aromatic hydrocarbon shorter ones [1]. The crushing of long chains of carbons into shorter chains in the catalytic cracking process is explained by the production of chemical reactions by a conjunction between the hydrocarbon molecules of the feed (carbocation formation) and the Brønsted

and Lewis acid sites of the zeolitic catalyst [2]. This carbocation can then undergo cracking to produce smaller molecules, isomerization to rearrange the molecules, and or hydrogen transfer to produce aromatic compounds [3]. However, because of the complexity of aromatic activated rings such as polyaromatic hydrocarbons, these can't be directly refined by the fluid catalytic cracking unit [4, 5].

Besides, in FCC feedstock cracking, several reactions occur during the process including hydrogen transfer between catalyst (hydrogen donor) and acceptors that can convert polyaromatic structures into less complex components, naphthene, and other aromatics. Even though, the hydrogen transfer is considered an undesirable reaction because it can also convert olefine into paraffin (lower octane number) [5, 6], is still important to decompose the polyaromatic hydrocarbon components and contribute to the production of environment-friendly valuable petroleum fractions.

The recent catalyst designers have tried to suppress the hydrogen transfer reaction [7, 8], but the problem that can be posed is the fate of the PAHs components conversion since several researchers reported that the catalyst's fast deactivation relates to them. Polyaromatic also known to be a major air pollutant depending on their concentrations in commercial products such as gasoline and diesel.

Therefore, understanding the catalyst behavior (deactivation and properties) and polyaromatic hydrocarbon conversions on an industrial scale is very important to obtain and optimize the heavy oil in the fluid catalytic cracking, specialty for the process where the residue atmospheric is immediately used without any pre-hydrotreatment [9, 10].

This present work firstly aims to demonstrate that aromatic and naphthene are the main cause of catalyst deactivation through a comparative study of fresh, regenerated, and spent catalyst states deeply characterized using BJH, FTIR, and NMR^{13}C methods under industrial FCC operating conditions. Secondly, aims to investigate the polyaromatic hydrocarbon conversion using the GC-MS method in the feedstock and reaction main product. The naphtha fraction (light cycle oil (LCO), with final boiling point (FBP)= 207°C and density (15°C) = g/cm^{-3}) was defined as the main reaction product, the sum of the LPG, Dry-gas, and coke products.

CRACKING MECHANISM BY HYDROGEN TRANSFER

Large amounts of alkenes should theoretically result from cracking reactions. However, this is untrue. It detects an alkene deficiency only because hydrogen from naphthenes or coke precursors transfers quickly to alkenes. The processes of hydrogen transfer and alkene protonation-deprotonation are involved one after the other. The nature and size distribution of the product hydrocarbons are significantly influenced by hydrogen transfer. The amount of alkanes and aromatics in the reaction products is increasing while the amount of alkenes and naphthenes is decreasing. The distribution is governed by the transformation of carbenium ions or olefins into alkanes, which are then broken down once again into light fractions [11].

The use of FAU zeolites in FCC catalysts, according to author Weisz [12], favors a greater ratio of hydrogen transfer rates and cracking, which in turn promotes the synthesis of aromatics and alkanes. Since zeolites are more active than silica-alumina, Gates et al. [13] observed that using them allowed for a reduction in the amount of catalyst needed. The high ratio for zeolites has been explained by Pine et al. [14], Scherzer [15], and Jacquinot et al. [16].

These include being relatively close to the proton acid sites of the zeolites, which significantly increases the transfer of hydrogen, a reaction that would require two acid sites for its catalysis [14] or is related to an extremely high concentration of reagents in the super-cages of the FAU [13] zeolites, which favors the bimolecular hydrogen transfer reaction over the monomolecular β scission reaction. Figure 1 shows an example of a PAH cracking mechanism in the presence of a hydrogen donor in a fluid catalytic cracking process.

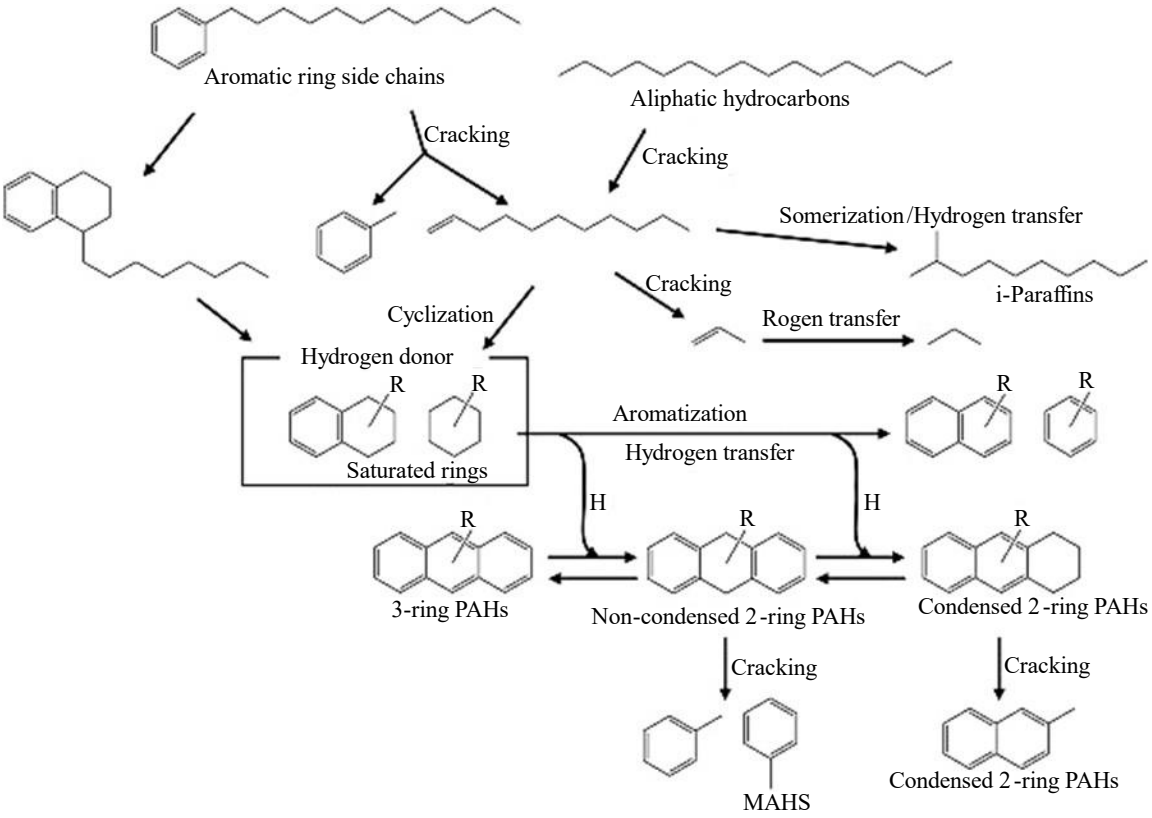

Figure 1. Typical three-ring cracking mechanism [17].

CATALYST DEACTIVATION

Fluid catalytic cracking deactivation during the process can be related to various causes but is classified into two categories. The first deactivation, namely reversible reactivation. This type of deactivation is caused by the pore clogging and surface recovery of the catalyst due to the deposition of carbon species during the reaction phase. However, it is easy to remove a considerably large amount of these deposited carbons and recover more than 50% of the catalyst activity, except for some aromatic and naphthene which are more complex and resistant to cracking. The second deactivation is named irreversible deactivation. This type is caused by particle thermal degradation, particle injection velocity or steam dealumination can be involved in the metals (vanadium, nickel, iron, sodium…) contaminations that react with catalyst particles and modify the catalyst structure: catalyst abrasion and fragmentation as shown.

RESULTS AND DISCUSSIONS

Barrett–Joyner–Halenda (BJH) analysis

Figure 2 displays the distributions of the pore width as a function of the volume and surface area. From the fresh catalyst to its spent state, it is observed major change during the fluid catalytic process as we demonstrated in our previous work [18]. According to the pore volume change, it can be observed from the curves that the fresh catalyst lost more than 50% of its volume in the first range of 0-160 Å due to the smaller pore clogging by hydrocarbon species [19]. It was also found that the pore volume of the spent catalyst doubled in the range of 160-295 Å while the regenerated catalyst pore volume increased from 295-466.78 Å. These changes correspond respectively the regions of particle fragmentation or other effects of the catalyst structure modification due to the thermal change [20].

Fourier-transform infrared (FTIR) analysis

Figure 3 shows the functional groups that exist on the zeolite's surface of fresh, regenerated, and spent catalysts. The 4000-400 cm^{-1} spectra revealed several peaks in all tested samples, some of them

were selected and assigned to their corresponding vibrations. The absorption bands of 3695.96 cm^{-1} and 3624.13 cm^{-1} that become more visible in the regenerated sample can be assigned to O-H stretching (free hydroxyl) [21]. These peaks were almost invisible in the fresh sample because the hydroxyl bonds linkage with zeolite structure are stable and still complex and in the spent sample the hydroxyl bonds were supposed to disappear due to the thermal decomposition of the catalyst during the FCC process. The lower absorption band of 1652.24 cm^{-1} that was revealed especially in the regenerated sample may be related to the C=N stretching. The bands of 1008.60 cm^{-1} and 448.37 cm^{-1} were presented in all samples and can be related to the functional groups of C=C bending alkene and υ(Xmetal-O) respectively. It manifested also two strong bands of 912.17 cm^{-1} and 532.26 cm^{-1} in the regenerated one. These peaks can be referred to the C-H_{OOP} aromatics and C-H bending respectively [22].

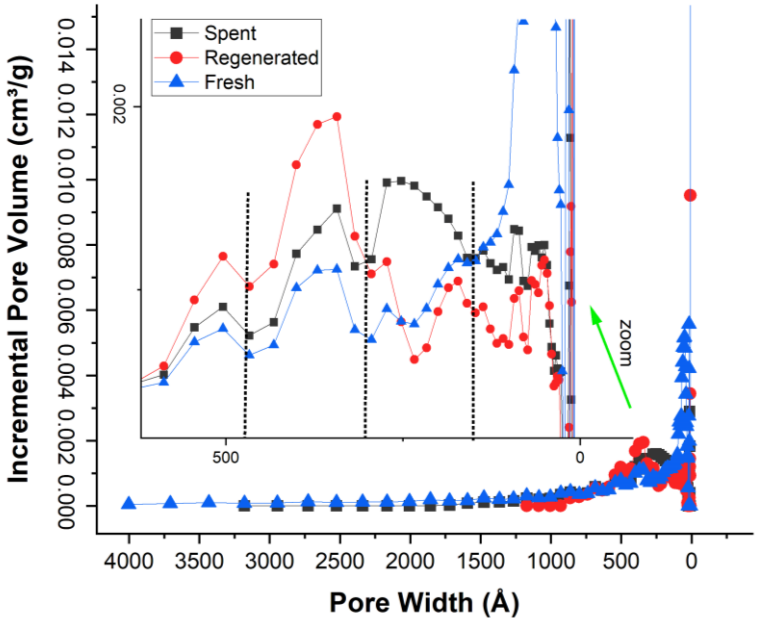

Figure 2. Pore volume distribution of the fresh, regenerated, and spent catalyst using Barrett–Joyner–Halenda (BJH).

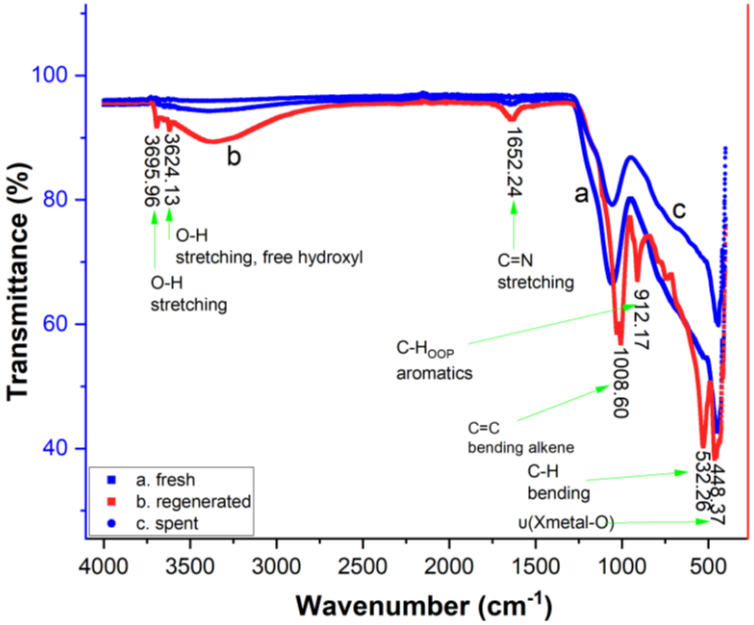

Figure 3. FTIR spectra of fresh, regenerated, and spent catalysts.

NMR^{13}C Analysis of Catalyst Deposited Coke Nature

Figure 4 shows 13C NMR spectra of the catalyst-deposited coke in its regenerated and spent states. The regenerated sample displayed four weak peaks of 171.20, 160.01, 65.45, and 44.59 ppm, while the spent sample showed only one strong peak of 125.24 ppm. The 65.45 and 44.59 peaks of the regenerated sample can be attributed to the aliphatic region (0-70), while the 171.20 and 160.01 ppm may be referred to as the aromatic region.

The spent sample's strong peak of 125.25 ppm [9] is located in the aromatic region (100-140). The results indicated a predominance of the aromatic species as the coke in the catalyst's internal structure. The spent catalyst result may be deduced that the aliphatic coke was transformed into aromatic hydrocarbon species.

PAHs Conversion

In implementing the sample extraction methodology, the rigorous USEPA method was adhered to using a sophisticated Focus GC model equipped with a highly sensitive FID (Buck M910 Buck Scientific USA) and a meticulously calibrated column measuring 30 m × 0.25 mm × 0.25 μm. Helium, serving as the carrier gas, flowed at a precise rate of 1.5 mL·min^{-1}, maintaining a column inlet split ratio of 1:5.

The temperature program initiated at 100°C for 1 minute, followed by a gradual increase at a rate of 25°C min^{-1} to 200°C. Further heating ensued at a rate of 40°C min^{-1}, reaching 300°C, where an isothermal state was maintained for 4.5 minutes. The injector temperature was meticulously set at 280°C, while the detector functioned seamlessly at 300°C.

For the solid phase in this investigative pursuit, C-18-bonded silica played a pivotal role in extracting PAH from the samples. A precisely measured 50 ml of each sample traversed a vacuum manifold housing 3g of methanol-dissolved silica gel at a consistent flow rate of 12 ml/min. The analytes adsorbed onto the silica underwent ethyl acetate elution, culminating in GC/FID analysis.

Identifying individual PAH residues within the samples was accomplished by applying identical GC analytical parameters, enabling a meticulous comparison of retention times with those acquired for the pesticide reference standard. This analytical approach ensures both precision and reliability in determining the composition of the samples under investigation.

Calculating the Residual PAHs

The peak area was used to assess the PAH residue levels. The detector's linear range was the confines of the measurement. To determine the concentration, the peak areas whose retention durations matched the standards were extrapolated on the matching calibration curves as presented in Figure 5 for each tested sample.

GC-MS Analysis

The feedstock analysis revealed a diverse range of aromatic hydrocarbons, initiating a thorough exploration into the transformation of these Polyaromatic Hydrocarbons (PAHs) across a resultant product. A meticulous GC-MS analysis of the feedstock, yielding an aromatic content of 18.3%, pinpointed specific polyaromatic components, including Fluorene, Flouranthene, Phenanthrene, Dibenzyl(a_h) anthracene, Anthracene, Acenaphthene, Benzo(k) fluoranthene, Benzo(a) pyrene, Xylene, Pyrene, Benzo(g_h_i) perylene, and Benzo(b) fluoranthene.

Among these, Flouranthene (five rings) and Phenanthrene (three rings) emerged as predominant PAHs in the feedstock, constituting 50.51% and 20.45%, respectively, of the total PAHs present. However, the impact of the cracking reaction on the polyaromatic hydrocarbons in the naphtha fraction revealed limited conversion, reaching only 25.70% of the total PAHs in the feedstock. This limitation was attributed to non-conversion and lower transformation rates of the main PAHs.

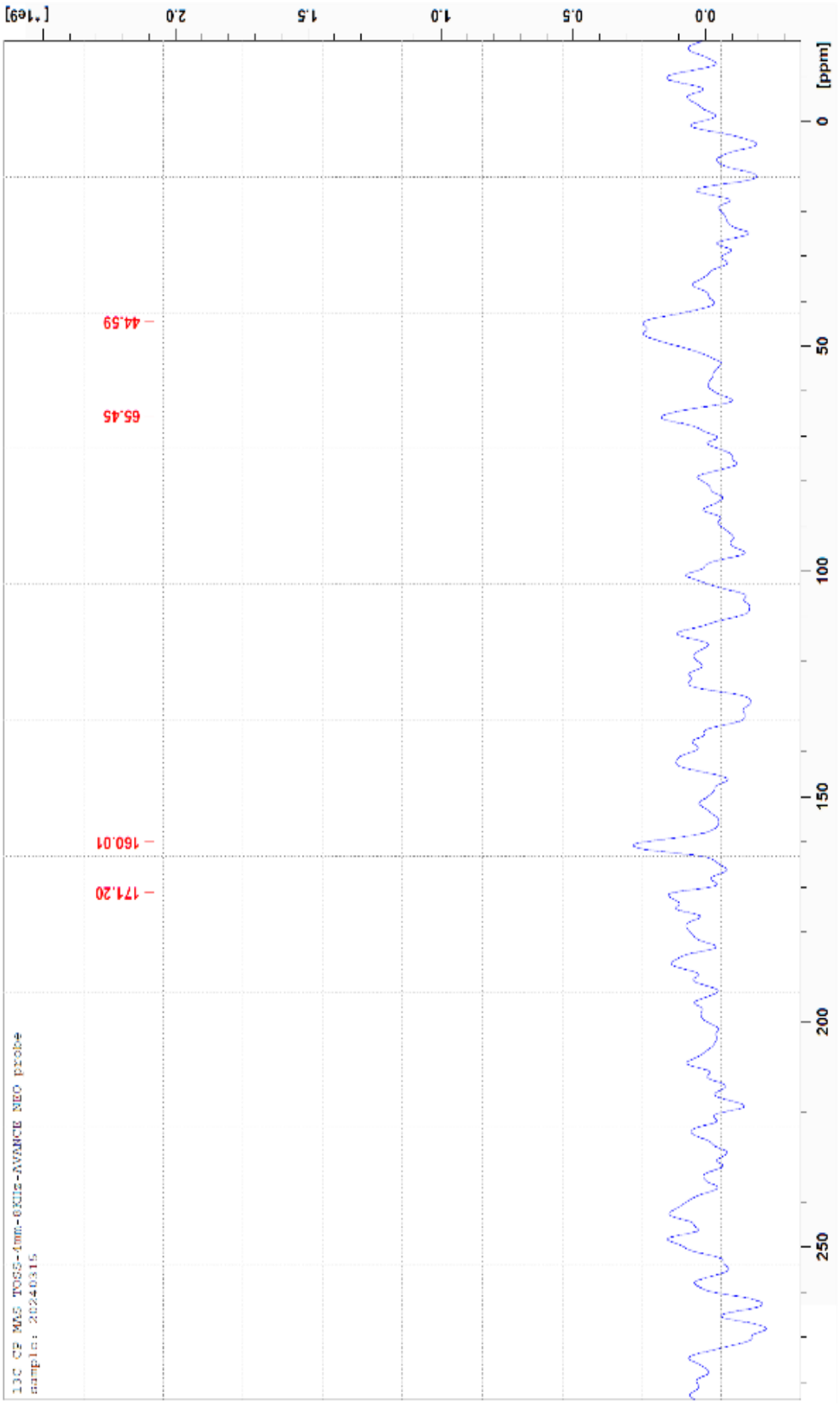

Figure 4. Nuclear magnetic resonance spectra of regenerated catalyst.

The detailed findings presented in Figure 6 underscored that only Flouranthene (4-rings), Phenanthrene (3-rings), Benzo(k) fluoranthene, and Xylene underwent conversion through hydrogen transfer in the fluid catalytic cracking reaction. Conversely, Benzo(b) fluoranthene, Benzo(g_h_i) perylene, Pyrene, Benzo(a) pyrene, Acenaphthene, Anthracene, Dibenzyl(a_h) anthracene, and Fluorene exhibited increased concentrations after cracking.

This nuanced understanding of PAH transformation offers valuable insights into the fluid catalytic cracking process and its implications for product composition.

For more efficient cracking of PAHs and their selectivity [1] in the FCC process, it is imperative to investigate the unit cell size (UCS) of the catalyst because this measurement takes into account the total number of tetrahedral aluminum sites which is responsible for hydrogen transfer reactions as reported by Galiano MC. et al. [23], de la Puente G. et al. [24], and Hernandez-Beltran, et al. [25].

Based on the above results, the four-ring (Flouranthene) and three-ring (Phenanthrene) predominated with more than 70% of the PAHs in the feedstock. The four-ring and three-ring catalyst cracking mechanisms were proposed in the literature [17]. With the presence of a hydrogen donor(catalyst), flouranthene and phenanthrene hydrocarbon molecules break down into smaller ones. The smaller hydrocarbon fragments desorb from the catalyst surface, releasing the cracked products as other products. These products may include smaller aromatic hydrocarbons, such as benzene, toluene, and xylenes。 Iori Shimada et al. [17] suggested a complex reaction mechanism of the three-rings PAH in the presence of hydrogen donor which can be described essentially as follows: Three-ring converted into two-rings by hydrogen reversible transfer rection.

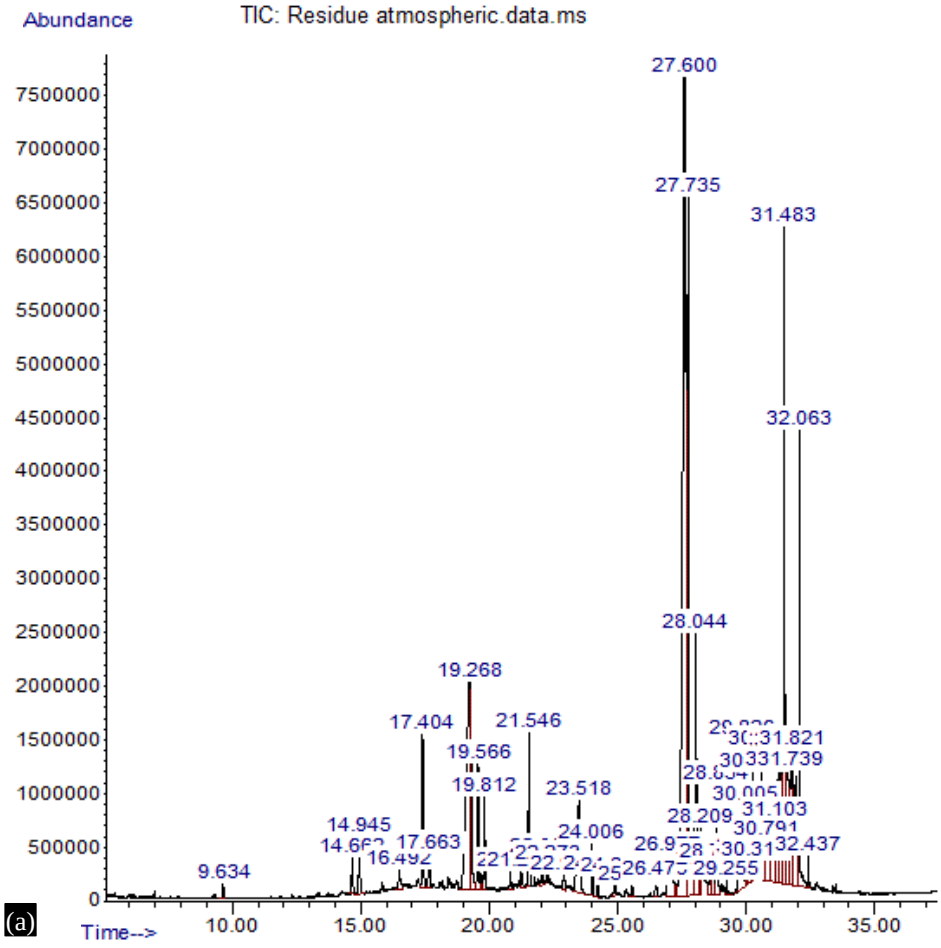

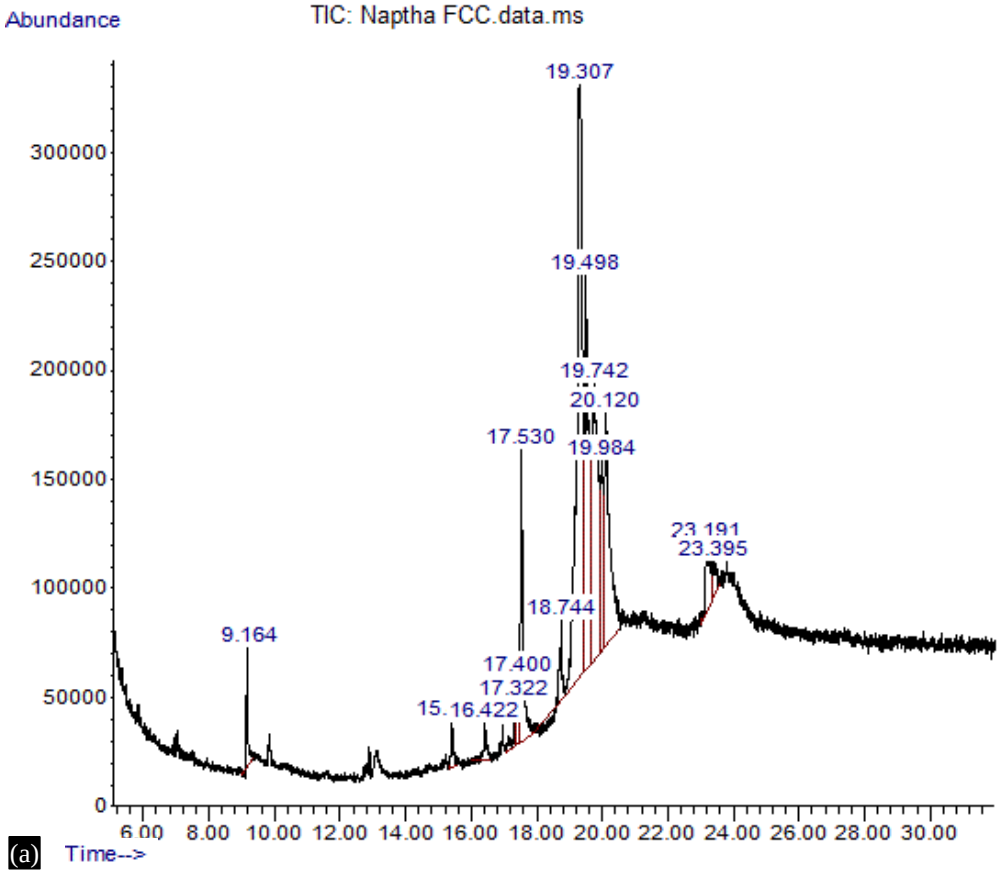

(a)

Figure 5. (a and b) Chromatograms of total ion flow from different tested samples.

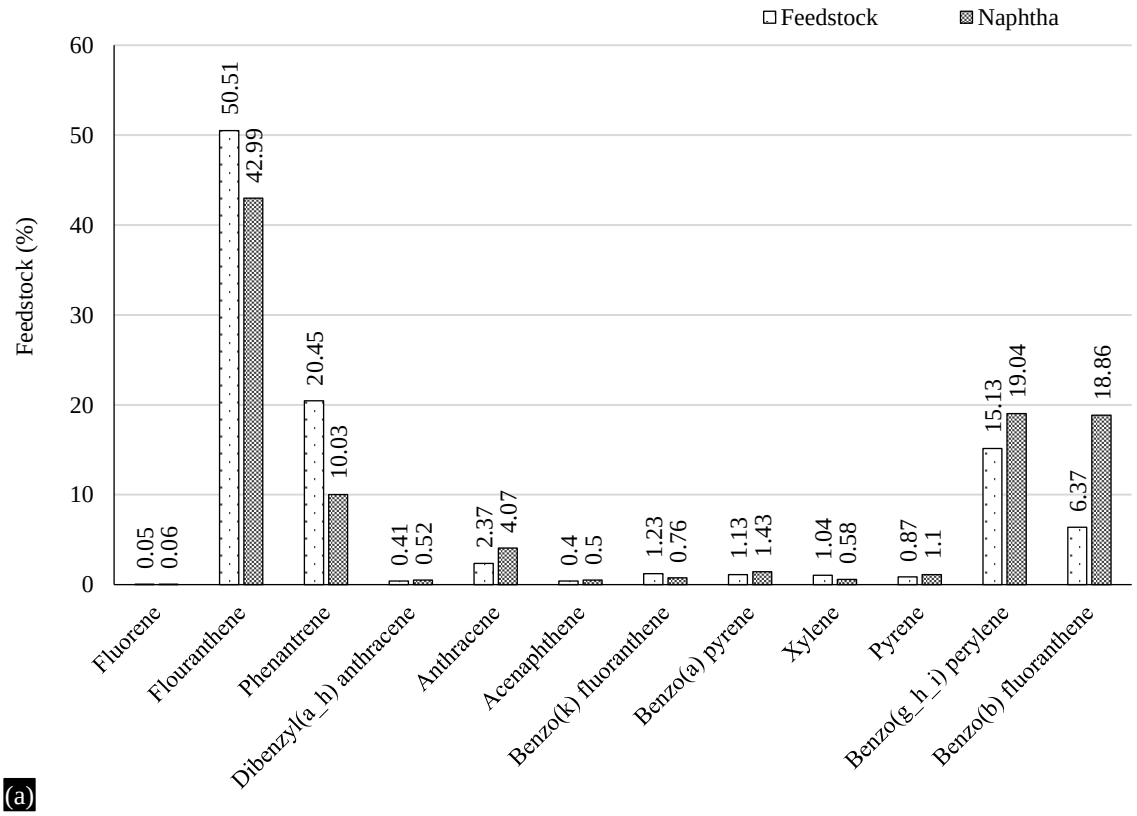

(a)

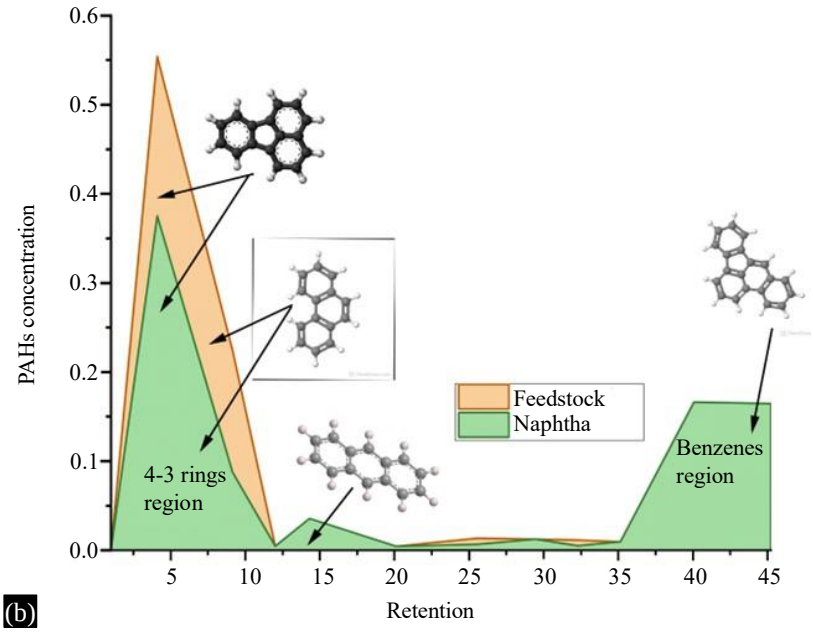

Figure 6. (a and b) Amount of each PAH in the feedstock and products.

Table 1. Catalyst properties [9].

Item	Density	Residual carbon	Weigh	Aromatics	Asphaltenes	Saturates	NSO
Unity	g/cm^3	wt.%	g/mol	wt.%	wt.%	wt.%	wt.%
value	0.921	5.5	462	18.34	7.10	33.44	41.12

Table 2. Feedstock properties [9].

Samples	S_{BET} (m^2g^{-1})	S_{ext} (m^2g^{-1})	S_{micro} (m^2g^{-1})	V_{total} (cm^3g^{-1})	V_{micro} (cm^3g^{-1})	Microporosity (%)
Fresh	158.13	94.24	63.8825	0.147	0.028	40.39
Regenerated	76.78	38.55	38.2327	0.098	0.017	49.79
Spent	57.45	28.87	28.5726	0.077	0.012	49.73

MATERIALS, METHODS, AND EXPERIENCES

Raw Materials

Solid Raw Materials

Equilibrium regenerated and spent catalysts recovery from Zinder Oil Refining Company. A fresh catalyst also was provided for a future comparison study of the catalyst deactivation causes and coke mechanism at different steps of the process that the operating conditions were described in our previous work given in Table 1.

Liquid Raw Materials

A non-hydrotreated atmospheric residue as a feedstock and Naphtha as light cycle oil (LCO, with final boiling point (FBP)= 207°C and density (15°C) =740.19 g/cm^{-3}) the process's main reaction product. Table 2 presents the feedstock properties [9] that were used over our equilibrium catalyst in this process.

Catalyst Characterization Methods

The catalyst behavior was studied in its fresh, regenerated, and spent states using several spectroscopy techniques. The pore volume distribution of all samples was calculated using the Barrett–Joyner–Halenda (BJH) method, and the isotherms conditions were detailed in our previous work [9].

Fourier-transform infrared (FTIR) technique was used to recognize the functional groups that exist on the surface of the catalyst, carbon species, and produced composite using the model Simfeuille IS50 spectrophotometer, 64 scan times, and resolution 4 cm^{-1}.

The nature of the hydrocarbon species or coke was recognized using Nuclear magnetic resonance ($NMR^{13}C$). the spectra were recorded on 13C CP MAS TOSS-4mm-8KHz-AVANCE NEO probe spectrometer model.

Experimental Section

In order to determine the polyaromatic hydrocarbons (PAHs) in feedstock and reaction product samples, a gas chromatography−mass spectrometry (GC-MS) analysis was carried out on Agilent Technologies GC system (GC-7890A/MS-5975C model) with an HP-5MS column (30 m length, 250 μm diameter, 0.25 μm film thickness). The electron ionization technique with high-energy electrons (70 eV) was utilized for GC-MS spectroscopic detection. Helium gas (99.99%) served as the carrier gas at a flow rate of 1 ml/min. The experimental conditions encompassed a 10-minute holding time, a temperature increase rate of 3°C/1 minute, and an initial temperature range of 50-150°C. The temperature range was set between 50 and 150°C initially, eventually reaching 300°C at a rate of 10°C/1 minute. Injection, performed splitless, involved the injection of 1% of the prepared extracts diluted with appropriate solvents. The relative amount (%) of chemical elements was then determined based on the peak area generated in the chromatogram, as elucidated in the discussion section.

PAHs conversion [%] = $(M_0 - M/M_0) \times 100$. Here, M0 and M represent the amount of the PAH element molar in the feedstock and reaction product, respectively.

CONCLUSION

In this section, an in-depth analysis was meticulously conducted employing a diverse array of spectroscopy techniques to scrutinize the intricate behavior of the equilibrium catalyst across three pivotal stages: fresh, regenerated, and spent stages. The detailed elucidation of catalytic deactivation was derived from a comprehensive examination of catalyst pore volume distribution and the presence of coke in the regenerated and spent catalyst states was confirmed by nuclear magnetic resonance spectroscopy ($NMR^{13}C$) result and revealed its nature as aromatic and aliphatic species. These multifaceted analyses brought to light the intricate coverage of the catalyst's active sites and the obstruction of its pores by aromatic and aliphatic species deposited during the process.

Fourier-transform infrared (FTIR) analysis of both spent and regenerated catalysts unveiled again the presence of polyaromatic species, including C=N stretching, C=C bending alkene, υ(Xmetal-O), C-HOOP aromatics, and C-H bending carbon structures.

A meticulous examination of polyaromatic hydrocarbons within the atmospheric residue (feedstock) revealed 12 distinct components. Significantly, the catalyst demonstrated selectivity in the conversion of these polyaromatic hydrocarbons, with some experiencing increased rates in reaction product (Naphtha)—a phenomenon attributed to the conversion of naphthene and olefin. This intricate exploration significantly advances our understanding of catalyst behavior and process dynamics, offering invaluable insights for the continual refinement of fluid catalytic cracking technologies in the pursuit of excellence. The development of new generation catalyst with specific unit cell size (UCS) selectivity of fluoranthene (4-rings) and phenanthrene(3-rings) (predominant PAHs in the non-hydrotreated atmospheric residue) may contribute to obtain light valuable commercial and proper products in this air of green energy politic.

REFERENCES

1. S. Suganuma, N. Katada, Selective Conversion of Polycyclic Aromatic Hydrocarbons for Formation of Valuable Chemicals from the Heavy Oil Component, Journal of the Japan Petroleum Institute 66 (2023) 95–100. https://doi.org/10.1627/JPI.66.95.

2. M. Guisnet, S. Mignard, Le craquage catalytique, unité clé d'une raffinerie, (2000).
3. A. Alkhlel, H. de Lasa, Catalyst/Feedstock Ratio Effect on FCC Using Different Catalysts Samples, Catalysts 2019, Vol. 9, Page 542 9 (2019) 542. https://doi.org/10.3390/CATAL9060542.
4. X. Dupain, E.D. Gamas, R. Madon, C.P. Kelkar, M. Makkee, J.A. Moulijn, Aromatic gas oil cracking under realistic FCC conditions in a microriser reactor☆, Fuel 82 (2003) 1559–1569. https://doi.org/10.1016/S0016-2361(03)00077-2.
5. F.N. Guerzoni, J. Abbot, Catalytic cracking of a binary mixture on zeolite catalysts, Appl Catal A Gen 103 (1993) 243–258. https://doi.org/10.1016/0926-860X(93)85055-T.
6. I. Shimada, K. Takizawa, H. Fukunaga, N. Takahashi, T. Takatsuka, Catalytic cracking of polycyclic aromatic hydrocarbons with hydrogen transfer reaction, Fuel 161 (2015) 207–214. https://doi.org/10.1016/J.FUEL.2015.08.051.
7. F.N. Guerzoni, J. Abbot, Catalytic cracking of a binary mixture on zeolite catalysts, Appl Catal A Gen 103 (1993) 243–258. https://doi.org/10.1016/0926-860X(93)85055-T.
8. M.C. Galiano, U.A. Sedran, Light Alkene Selectivity on Y Zeolite FCC Catalysts, Ind Eng Chem Res 36 (1997) 4207–4211. https://doi.org/10.1021/IE960510V.
9. S.Y. Zakariyaou, H. Ye, A.D.M. Oumarou, M.S. Abdoul Aziz, S. Ke, Characterization of Equilibrium Catalysts from the Fluid Catalytic Cracking Process of Atmospheric Residue, Catalysts 2023, Vol. 13, Page 1483 13 (2023) 1483. https://doi.org/10.3390/CATAL13121483.
10. H. Li, S. Li, J. Wu, L. Xie, Y. Liang, Y. Zhang, S. Zhao, C. Xu, Q. Shi, Molecular characterization of aromatics in petroleum fractions by combining silica sulfuric acid sulfonation with electrospray ionization high-resolution mass spectrometry, Fuel 317 (2022) 123463. https://doi.org/10.1016/J.FUEL.2022.123463.
11. H. Li, S. Li, J. Wu, L. Xie, Y. Liang, Y. Zhang, S. Zhao, C. Xu, Q. Shi, Molecular characterization of aromatics in petroleum fractions by combining silica sulfuric acid sulfonation with electrospray ionization high-resolution mass spectrometry, Fuel 317 (2022) 123463. https://doi.org/10.1016/J.FUEL.2022.123463.
12. Zeolites: Science and Technology, Zeolites: Science and Technology (1984). https://doi.org/10.1007/978-94-009-6128-9.
13. B.C. Gates, J.R. (James R. Katzer, G.C.A. Schuit, Chemistry of catalytic processes, (1979) 464. https://books.google.com/books/about/Chemistry_of_Catalytic_Processes.html?id=FsFTAAAAMAAJ (accessed January 10, 2024).
14. L.A. Pine, P.J. Maher, W.A. Wachter, Prediction of cracking catalyst behavior by a zeolite unit cell size model, J Catal 85 (1984) 466–476. https://doi.org/10.1016/0021-9517(84)90235-5.
15. Jr. W C Kittler, A. Argoitia, P.G. Coombs, C.T. Markantes, non-toxic flakes for authentication of pharmaceutical articles, (2009). https://books.google.com/books/about/Octane_Enhancing_Zeolitic_FCC_Catalysts.html?id=0R2qSCsVT3cC (accessed January 10, 2024).
16. Zeolite Microporous Solids: Synthesis, Structure, and Reactivity, Zeolite Microporous Solids: Synthesis, Structure, and Reactivity (1992). https://doi.org/10.1007/978-94-011-2604-5.
17. I. Shimada, C. Uno, Y. Watanabe, T. Takatsuka, Catalytic cracking of three-ring polycyclic aromatic hydrocarbons in the presence of hydrogen donors, Fuel Processing Technology 232 (2022) 107267. https://doi.org/10.1016/J.FUPROC.2022.107267.
18. S.Y. Zakariyaou, H. Ye, A.D.M. Oumarou, M.S. Abdoul Aziz, S. Ke, Characterization of Equilibrium Catalysts from the Fluid Catalytic Cracking Process of Atmospheric Residue, Catalysts 13 (2023) 1483. https://doi.org/10.3390/catal13121483.
19. J. Goetze, F. Meirer, I. Yarulina, J. Gascon, F. Kapteijn, J. Ruiz-Martínez, B.M. Weckhuysen, Insights into the Activity and Deactivation of the Methanol-to-Olefins Process over Different Small-Pore Zeolites As Studied with Operando UV-vis Spectroscopy, ACS Catal 7 (2017) 4033–4046. https://doi.org/10.1021/acscatal.6b03677.
20. F. Krumeich, J. Ihli, Y. Shu, W.C. Cheng, J.A. Van Bokhoven, Structural Changes in Deactivated Fluid Catalytic Cracking Catalysts Determined by Electron Microscopy, ACS Catal 8 (2018) 4591–4599. https://doi.org/10.1021/acscatal.8b00649.

21. B. Hazra, A.K. Varma, A.K. Bandopadhyay, S. Chakravarty, J. Buragohain, S.K. Samad, A.K. Prasad, FTIR, XRF, XRD and SEM characteristics of Permian shales, India, J Nat Gas Sci Eng 32 (2016) 239–255. https://doi.org/10.1016/j.jngse.2016.03.098.
22. Y. Ruiz-Morales, A.D. Miranda-Olvera, B. Portales-Martínez, J.M. Domínguez, Determination of13C NMR Chemical Shift Structural Ranges for Polycyclic Aromatic Hydrocarbons (PAHs) and PAHs in Asphaltenes: An Experimental and Theoretical Density Functional Theory Study, Energy and Fuels 33 (2019) 7950–7970. https://doi.org/10.1021/acs.energyfuels.9b00182.
23. M.C. Galiano, U.A. Sedran, Light Alkene Selectivity on Y Zeolite FCC Catalysts, Ind Eng Chem Res 36 (1997) 4207–4211. https://doi.org/10.1021/IE960510V.
24. G. De La Puente, U. Sedran, Conversion of methylcyclopentane on rare earth exchanged Y zeolite FCC catalysts, Appl Catal A Gen 144 (1996) 147–158. https://doi.org/10.1016/0926-860X(96)00115-9.
25. F. Hernández-Beltrán, J.C. Moreno-Mayorga, M. De Lourdes Guzmán-Castillo, J. Navarrete-Bolaños, M. González-González, B.E. Handy, Dealumination–aging pattern of REUSY zeolites contained in fluid cracking catalysts, Appl Catal A Gen 240 (2003) 41–51. https://doi.org/10.1016/S0926-860X(02)00433-7.

